

# Nodal/Antinodal Dichotomy and the Energy-Gaps of a doped Mott Insulator

M. Civelli<sup>1</sup>, M. Capone<sup>2</sup>, A. Georges<sup>3</sup>, K. Haule<sup>4</sup>, O. Parcollet<sup>5</sup>, T. D. Stanescu<sup>6</sup>, and G. Kotliar<sup>4</sup>

<sup>1</sup> *Theory Group, Institut Laue Langevin, Grenoble, France*

<sup>2</sup> *SMC, CNR-INFM, and Physics Department, University of Rome "La Sapienza", Piazzale A. Moro 5, I-00185, Rome, Italy and Istituto dei Sistemi Complessi, Via dei Taurini 19, I-00185, Rome, Italy*

<sup>3</sup> *Centre de Physique Théorique, Ecole Polytechnique, 91128 Palaiseau Cedex, France*

<sup>4</sup> *Physics Department and Center for Materials Theory, Rutgers University, Piscataway NJ USA*

<sup>5</sup> *Service de Physique Théorique, CEA/DSM/SPHT-CNRS/SPM/URA 2306 CEA-Saclay, F-91191 Gif-sur-Yvette, France and*

<sup>6</sup> *Condensed Matter Theory Center, Department of Physics, University of Maryland, College Park, Maryland 20742-4111, USA*

(Dated: November 24, 2018)

Using Cellular Dynamical Mean Field Theory with exact diagonalization as the impurity solver we study the superconducting state of the hole-doped two-dimensional Hubbard model. In the underdoped regime, the formalism leads to a natural decomposition of the photoemission energy-gap into two components. The first gap, stemming from the anomalous self-energy, dominates near the nodes and decreases with decreasing doping. The second gap has an additional contribution from the normal self-energy inherited from the normal-state pseudo-gap. It is dominant near the antinodes and increases as the Mott insulating phase is approached.

PACS numbers: 71.10.w, 71.10.Fd, 74.20.z, 74.72.h

Superconductivity of strongly correlated materials such as the high- $T_c$  cuprates (HTCS) and the theoretical models describing this phenomenon have been subject of intensive research for more than twenty years (for a review see, e.g., [1]). Starting from the weak correlation limit (realized for large doping or small interaction strength), effective low-energy descriptions in terms of Fermi liquid quasi-particles interacting with collective excitations, such as phonons and spin fluctuations, have been intensively studied. A different approach views the essence of the HTCS phenomenon as deriving from the proximity to a parent strongly-interacting Mott insulator. In this framework, superconductivity is the result of introducing holes into a spin liquid state [2]. The strong correlation viewpoint has not been yet developed into a fully quantitative theory and whether the weak- and strong-coupling pictures are qualitatively or only quantitatively different is an important open issue.

The development of Dynamical Mean Field Theory (DMFT) and its cluster extensions [3] provide a new path to investigate strongly correlated electron models. These methods aim to build a mean field theory for Hubbard-like models using a cluster of sites embedded in a self-consistent bath. The Hubbard model at relatively small interaction strength ( $U \leq 4t$ ) has been extensively investigated using very large clusters by means of the Dynamical Cluster Approximation. The ensuing d-wave superconductivity is well described by an exchange of spin fluctuations [4]. The Mott transition has been studied from the strong coupling end ( $U \geq 8t$ ) by many groups. Qualitatively interesting phenomena were identified, such as the competition of an anomalous superconducting state [5] with antiferromagnetism [6], the presence of a pseudogap [7, 8], the formation of Fermi arcs [9, 10] and the existence of an avoided critical point [11]. In

this work we use CDMFT to explore the nature of the energy-gap in the one-particle spectra when correlations are strong. The goal is to explore the qualitative aspects that characterize the approach to the Mott transition in the light of recent studies reporting the presence of two different energy scales in the nodal and antinodal regions in the superconducting state of the cuprates [12, 13].

We focus on the one-band two-dimensional Hubbard Model as a minimal description of the doping-driven Mott transition :

$$\mathcal{H} = - \sum_{\langle i,j \rangle, \sigma} t_{ij} (c_{i,\sigma}^\dagger c_{j,\sigma} + h.c.) + U \sum_i n_{i\uparrow} n_{i\downarrow} - \mu \sum_i n_i, \quad (1)$$

where  $c_{i,\sigma}$  ( $c_{i,\sigma}^\dagger$ ) are destruction (creation) operators for electrons of spin  $\sigma$ ,  $n_{i\sigma} = c_{i\sigma}^\dagger c_{i\sigma}$  is the number operator,  $U$  is the on-site repulsion and  $\mu$  the chemical potential. Throughout the paper the next-nearest-neighbor hopping is  $t' = -0.3t$  and the Hubbard repulsion  $U = 12t$ . We implement CDMFT on a  $2 \times 2$  plaquette, which allows to study the d-wave superconducting state [5].  $\mathcal{H}$  is mapped onto a  $2 \times 2$ -cluster Anderson impurity model, in which an interacting plaquette is embedded in a self-consistent non-interacting bath. The impurity model is solved using the Exact Diagonalization method [15], enforcing the CDMFT self-consistency condition

$$\hat{\mathcal{G}}(i\omega_n)^{-1} = (\hat{G}[\hat{\Sigma}])^{-1}(i\omega_n) + \hat{\Sigma}(i\omega_n) \quad (2)$$

$$\hat{G}[\hat{\Sigma}](i\omega_n) = \sum_K \left[ (i\omega_n + \mu) \hat{1} - \hat{t}(K) - \hat{\Sigma}(i\omega_n) \right]^{-1},$$

where the hat denotes  $8 \times 8$  matrices with cluster-site indices containing both normal and anomalous components (Nambu notation).  $\hat{\mathcal{G}}$  is the “Weiss field” describing the bath,  $\hat{t}(K)$  is the hopping-matrix written in su-

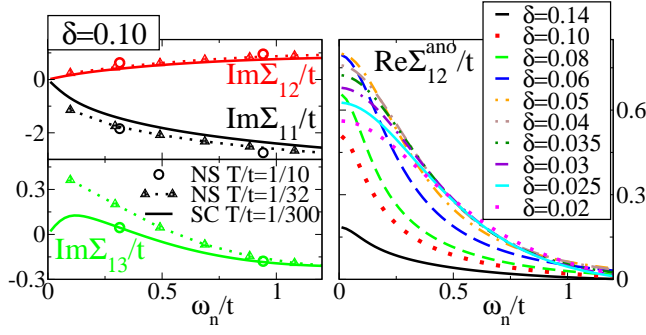


FIG. 1: (Color online). Cluster self-energies in Matsubara frequencies. Left panels: the normal components of  $\text{Im}\hat{\Sigma}$  (in the top the local  $\text{Im}\hat{\Sigma}_{11}$  and nearest-neighbor  $\text{Im}\hat{\Sigma}_{12}$ , in the bottom the next-nearest-neighbor  $\text{Im}\hat{\Sigma}_{13}$ ) in the superconducting solution (SC,  $T = 1/300t$ ) are compared with the normal-state (NS) results at higher virtual temperatures ( $T = 1/10t$  and  $T = 1/32t$ ), for doping  $\delta = 0.1$ . Right panel: Real part of the anomalous self-energy  $\text{Re}\Sigma_{12}^{\text{ano}}$  as a function of doping.

percell notation with  $K$  restricted to the reduced Brillouin zone, and  $\hat{\Sigma}$  is the cluster self-energy, the output of the impurity solver. These relations are imposed on the Matsubara frequency axis at low virtual temperature  $T = 1/300t$ , by fitting the bath spectral function in the energy-interval up to  $\sim 2U$  with a truncated 8-pole function and weighting more the low-energy part[3].

In Fig. 1 we plot normal and anomalous components of the cluster self-energy  $\hat{\Sigma}$  on the Matsubara axis. In the left panels, we compare the imaginary parts of the normal component of  $\hat{\Sigma}$  for a given doping  $\delta = 0.1$  with the corresponding normal-state results at a higher virtual temperature. We remark that we have not been able to obtain normal-state CDMFT solutions at very low temperatures in a finite range of doping around  $\delta = 0.1$ . In the superconducting case (full line), all the imaginary parts of the cluster self-energies vanish linearly at small frequency, i.e., our cluster solution has a Fermi liquid-type character. This is substantially different from the high-virtual- $T$  normal-state solution (circles  $T = 1/10$ , triangles  $T = 1/32$ ). In a Fermi liquid in fact, the intercepts of  $\text{Im}\Sigma$  scale as  $T^2$ . However, in the temperature range accessible by the normal-state calculation, the next-nearest-neighbor  $\text{Im}\Sigma_{13}$  (bottom panel) violates the Fermi liquid behavior by increasing as  $T$  decreases[8]. We show the anomalous component of the cluster self-energy on the Matsubara axis in the right panel of Fig. 1. Only the nearest-neighbors  $\text{Re}\Sigma_{12}^{\text{ano}}$  is appreciably non-zero and it presents a non-monotonic behavior at small frequency, as we move from the overdoped ( $\delta < 0.08$ ) to the underdoped ( $\delta > 0.08$ ) side. This influences the energy-gap properties of the system in a fundamental way, as we will discuss in the following.

In order to extract momentum-dependent quantities within CDMFT, we need a periodization procedure which

restores the translational symmetry. Several methods have been discussed in the literature[3]. Near the nodal point  $k \sim (\frac{\pi}{2}, \frac{\pi}{2})$ , we find that well defined nodal quasi-particle are described by a regular self-energy which is extracted from the cluster self-energies via:

$$\Sigma_{\sigma}(k, \omega) = \frac{1}{N_c} \sum_{\mu\nu} e^{-ik\mu} \Sigma_{\mu\nu, \sigma}(\omega) e^{ik\nu} \quad (3)$$

where  $\mu, \nu$  label the  $N_c$  cluster sites. In this gapless region the anomalous self-energy determines the physics and it acquires a standard  $d_{x^2-y^2}$ -wave form:  $\Sigma^{\text{ano}}(k, \omega) = \Sigma_{12}^{\text{ano}}(\omega) (\cos k_x - \cos k_y)$ . In the antinodal region the normal component of the self-energy is very large and a pseudogap forms in the one-particle spectrum as we approach the Mott insulator (see below). In this situation, we exploit the fact that the normal component of the irreducible two-point cumulant  $\mathcal{M}_{\sigma}^{\text{nor}}(k, \omega)$  has a regular behavior at low energy[10] and can be obtained by periodizing the cluster-cumulants, i.e. applying Eq. (3) to  $\hat{\mathcal{M}}_{\sigma}^{\text{nor}} = [(\omega + \mu)\hat{1} - \hat{\Sigma}_{\sigma}^{\text{nor}}]^{-1}$ . The momentum-dependent normal component of the self-energy is obtained from  $\Sigma^{\text{nor}}(k, \omega) = [\omega + \mu - (\mathcal{M}_{\sigma}^{\text{nor}}(k, \omega))^{-1}]^{-1}$ . This procedure is able to describe the physics of the antinodal region of momentum space, where the spectral function is incoherent and quasi-particles not well defined, as observed in photoemission experiments (e.g. in Ref.[16] and chap. 3 in Ref.[1]). We have checked that this periodization reconstructs the local Green's function (upon integrating the lattice Green's function in momentum space) much better than the periodization of  $\hat{\Sigma}$  or  $\hat{\mathcal{M}}$  alone. We can now express the momentum-dependent Green's function. Defining the free particle spectrum  $\varepsilon_k \equiv t_k - \mu$ , we obtain a  $2 \times 2$  matrix Green's function in Nambu space

$$G_{k\sigma}^{-1}(\omega) = \begin{pmatrix} \omega - \varepsilon_k - \Sigma_{\sigma}^{\text{nor}}(k, \omega) & -\Sigma^{\text{ano}}(k, \omega) \\ -\Sigma^{\text{ano}}(k, \omega) & \omega + \varepsilon_k + \Sigma_{\sigma}^{\text{nor}}(k, -\omega)^* \end{pmatrix} \quad (4)$$

The diagonal entry  $G_{\sigma}^{11}(k, \omega)$  is the normal component, whose imaginary part is proportional to the spectral function, observable in photoemission spectroscopy.

In order to disentangle the normal component contribution to the spectral function  $A(k, \omega) = -\frac{1}{\pi} \text{Im}G_{\sigma}^{11}(k, \omega)$ , we first set  $\Sigma^{\text{ano}} = 0$  in Eq. (4). We present these results in Fig. 2 where  $A(k, \omega)$  is plotted for different dopings at two different locations in the Brillouin zone, representative of the nodal (panel A) and the antinodal (panel B) regions. We adopt the experimental procedure of Ref.[13] and determine the nodal and antinodal  $k$ -points as those where a quasi-particle peak of maximal height is observed (which at low doping in the antinodes can be situated at negative frequency). Their location as a function of doping is shown in the inset of panel C. Near the nodal point a quasi-particle peak is well defined at the Fermi level ( $\omega = 0$ ) and decreases by decreasing doping. In the antinodal region,

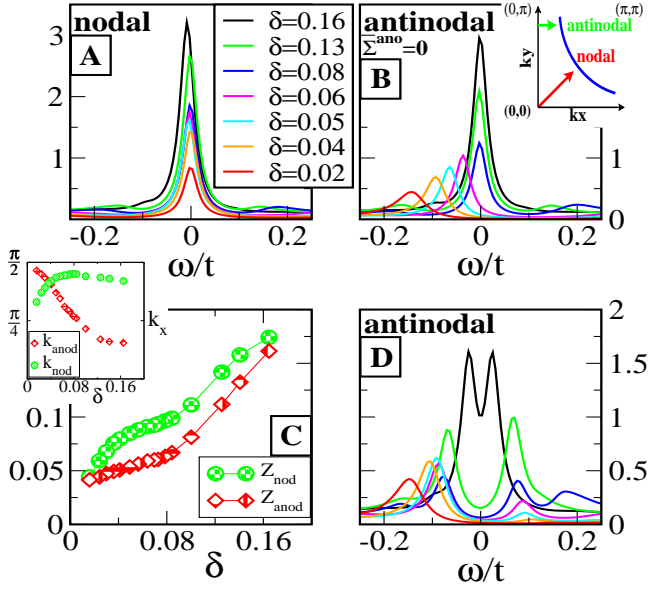


FIG. 2: (Color online) Evolution of the spectral function  $A(k, \omega)t$  with doping. Panel A, nodal quasi-particle peak; Panel B, normal component (set  $\Sigma^{\text{ano}} = 0$  in Eq. (4)) of the antinodal quasi-particle peaks; Panel C, nodal and antinodal quasi-particle weights. The inset shows the  $k$ -positions of the nodal and antinodal points; Panel D, spectra at the antinodes.

a quasi-particle peak is also found at the Fermi level for  $\delta > 0.08$ . For  $\delta < 0.08$ , however, the renormalized quasi-particle dispersion  $\xi_k^0 \equiv \varepsilon_k + \text{Re}\Sigma^{\text{nor}}(k, 0)$  never reaches zero along the line from  $(0, \pi) \rightarrow (\pi, \pi)$ , and the spectral weight shifts to negative energies signaling the opening of a pseudogap (PG). This feature has already been identified in normal-state studies[10]. The magnitude of the PG increases further with decreasing doping. At the same time the peak at the edge of the PG decreases and broadens by approaching the Mott insulator indicating that at the antinodes the physics becomes more and more incoherent. The approach to the Mott transition is thus characterized by a strong reduction in the area of the spectral peaks. We denote this area by  $Z$  and plot it in panel C. The nodal ( $Z_{\text{nod}}$ ) and antinodal ( $Z_{\text{anod}}$ ) weights decrease as we lower doping. However, we cannot rule out the possibility that they extrapolate to a finite but very small value at the transition. Moreover, in the underdoped region the quasi-particle weight displays a momentum-space modulation, being  $Z_{\text{nod}} > Z_{\text{anod}}$ [17]. In panel D, we switch on superconductivity by restoring  $\Sigma^{\text{ano}}$ . The superconducting gap opens in the antinodal region (the nodal region is practically unaffected). While for  $\delta > 0.08$  this results in spectra which are almost symmetric around the Fermi level, as in a standard BCS d-wave superconductor, close to the Mott transition the underlying PG, which originates from the normal component, superimposes to the superconducting gap resulting in asymmetric spectra.

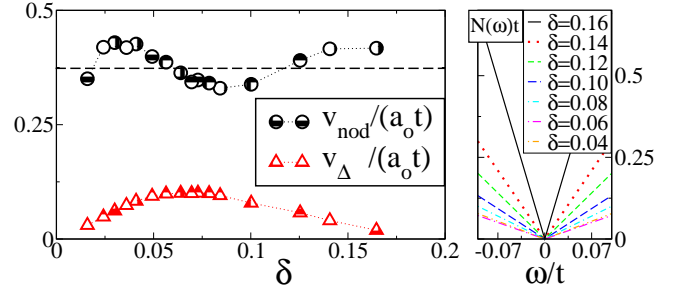


FIG. 3: (Color online) Left: nodal  $v_{\text{nod}}$  and anomalous  $v_{\Delta}$  velocities as a function of doping  $\delta$  ( $a_o$  denotes the lattice spacing). Right: evolution with doping of the low-energy local density of states  $N(\omega)t$ .

In the nodal region, the quasi-particles are well defined at all dopings and we can perform the standard Landau Fermi-liquid analysis by expanding the self-energies in Eq. (4) at low frequencies. We checked that the quasi-particle residue  $(1 - \partial_{\omega} \text{Re}\Sigma_k(\omega))^{-1}|_{\omega=0}$  numerically coincides with the area of the quasi-particle peak  $Z_{\text{nod}}$  shown in panel C of Fig. 2. From Eq. (4), we get  $A(k, \omega) \simeq Z_{\text{nod}} \delta \left( \omega - \sqrt{v_{\text{nod}}^2 k_{\perp}^2 + v_{\Delta}^2 k_{\parallel}^2} \right)$ , where  $v_{\text{nod}} = Z_{\text{nod}} |\nabla_k \xi_k^0|$  is the quasi-particle Fermi velocity perpendicular to the Fermi surface and  $v_{\Delta} = Z_{\text{nod}} |\nabla_k \Sigma^{\text{ano}}(k)|$  is the anomalous velocity parallel to the Fermi surface. Tunneling experiments measure the local density of states  $N(\omega) = -\frac{1}{\pi} \sum_k \text{Im} G_{\sigma}^{11}(k, \omega) \sim \frac{1}{\pi} \frac{Z_{\text{nod}}}{v_{\text{nod}} v_{\Delta}} \omega$  for small frequencies. This observable, as well as, e.g., the specific heat and the thermal conductivity of the superconductor, have simple expressions in terms of quantities that can be extracted from the low-energy expansion of the Green's function. On the left side of Fig. 3 the nodal  $v_{\text{nod}}$  and anomalous  $v_{\Delta}$  velocities are displayed as a function of doping.  $v_{\text{nod}}$  shows a roughly constant trend compatible with the experiments on cuprates[18]. The anomalous velocity  $v_{\Delta} \ll v_{\text{nod}}$  presents a dome-like shape in going from the overdoped to the underdoped region. Notice that  $v_{\Delta}$  measures the slope of the superconducting gap at the node. Its behavior, reported here (and confirmed by continuous time quantum Monte Carlo calculations[19]), is in agreement with recent experiments on underdoped cuprate materials which have shown that, contrary to the antinodal gap, the nodal superconducting gap decreases by reducing doping[12, 13]. Taking now  $Z_{\text{nod}}$  from Fig. 2, the slope of local density of states  $N(\omega)$  is calculated and displayed in the right panel of Fig. 3. The slope is monotonically decreasing by decreasing doping from the overdoped to the underdoped side of the phase diagram, and eventually becomes roughly constant at very low doping in agreement with scanning tunneling microscopy results[20].

We finally turn to the analysis of the one-electron spectra in the antinodal region, shown in Fig. 4. We eval-

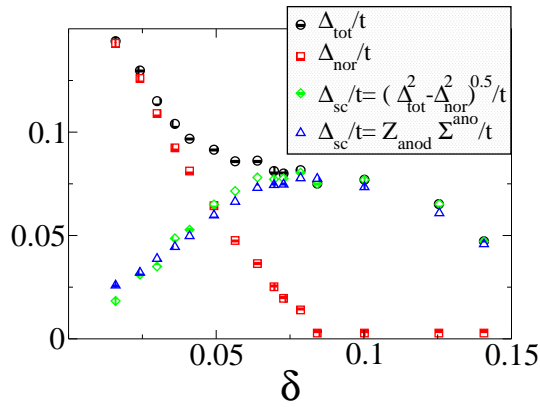


FIG. 4: (Color online) Antinodal energy gap  $\Delta_{tot}$  (circles), obtained from the spectra of panel D in Fig. 2, as a function of doping  $\delta$ , and decomposed in a normal contribution  $\Delta_{nor}$  (squares), obtained from panel B in Fig. 2, and in a superconducting contribution  $\Delta_{sc}$  (diamonds).

uated the antinodal gap in the superconducting state  $\Delta_{tot}$  by measuring the distance from the Fermi level ( $\omega = 0$ ) at which spectral peaks are located (panel D of Fig. 2).  $\Delta_{tot}$  monotonically increases by reducing doping, as observed in experiments on HTCS. At small doping, a PG opens at a critical doping  $\delta_c \approx 0.08$ . In order to disentangle the contribution of the normal component from the superconducting gap, we look at panel B of Fig. 2, where we have set  $\Sigma^{ano} = 0$ . While we are able to identify (at a finite frequency  $\omega_{pg} < 0$ ) a peak in the spectrum, this may not correspond strictly speaking to a Landau quasi-particle, since it can decay into the lower-energy nodal quasi-particles. The weight of such a peak,  $Z_{anod}$ , displayed in panel C of Fig. 2 does not necessarily correspond to a Fermi-liquid quasi-particle renormalization. As with  $\Delta_{tot}$ , we define the normal contribution to the antinodal energy-gap  $\Delta_{nor} = |\omega_{pg}|$  from panel B of Fig. 4. We also isolate and display the anomalous contribution to the total antinodal gap  $\Delta_{sc} = \sqrt{\Delta_{tot}^2 - \Delta_{nor}^2}$  and find that, within our numerical accuracy  $\Delta_{sc}(k) \sim Z_{anod}|\Sigma^{ano}(k, 0)|$ . The appearance of a finite  $\Delta_{nor}$  coincides with a downturn in  $\Delta_{sc}$ . We interpret  $\Delta_{tot}$  as the monotonically increasing antinodal gap observed in cuprates superconductors, while the superconducting gap  $\Delta_{sc}$ , detectable as the nodal-slope  $v_\Delta$  (Fig. 3), is decreasing in approaching the Mott transition.

The concept of two energy gaps with distinct doping dependence in the high temperature superconductors has recently been brought into focus from an analysis of Raman spectroscopy[12], and photoemission experiments[13] [14]. Here we show that this observation follows naturally from the simplest (dynamical) mean field treatment of correlated superconductivity near a Mott transition with strong antiferromagnetic correla-

tions. Notice that the one particle gap in the CDMFT picture is unusual. It is the result of *both* the anomalous self-energy and the normal self-energy. This is reminiscent of the earlier slave boson mean field treatment of the t-J model[21, 22], which uses order parameters defined within a plaquette and includes the possibility of pairing in *both* the particle-particle and the particle-hole channels. Compared to the self-energy of the slave boson treatment, as in the Resonating Valence Bond (RVB) treatment[22], the CDMFT lattice-self-energy has relevant normal and anomalous components at small doping, it has considerably stronger variations on the Fermi surface[10] and additional frequency dependence, which makes the one electron states near the antinodal point very incoherent even in the superconducting state. Furthermore, in the RVB slave boson mean field theory the anomalous self-energy of the electron increases with decreasing doping, in contrast to our findings in CDMFT.

Finally, we note that, as we have not been able to converge a normal state CDMFT solution at very low effective temperatures, we cannot address the seemingly contradictory results on a non-superconductive ground-state of Ref.[23], as discussed in Ref.[24]. It is possible that, just like in cuprates, additional fields or perturbations need to be applied to the mean field theory in order to be able to stabilize a "normal" state down to zero temperature.

We thank E.Katz, P.Nozières, P.Phillips, C.Castellani, A.-M. Tremblay, B.Kyung and S.S. Kancharla for useful discussions. M.Ca. acknowledges financial support by MIUR PRIN05 and by CNR-INFN, G.K. was supported by the NSF under Grant No. DMR 0528969.

- 
- [1] "Physics of Superconductors II", K. H. Bennemann and J. B. Ketterson, Springer-Verlag Berlin Heidelberg New York (2004).
  - [2] P.W. Anderson, Science **235**, 1196 (1987).
  - [3] For reviews see: A. Georges *et al.*, Rev. of Mod. Phys. **68**, 13 (1996); A.-M.S. Tremblay *et al.*, Low Temp. Phys., **32**, 561-595 (2006); Th. Maier *et al.*, Rev. of Mod. Phys. **77**, 1027-1080 (2005); G. Kotliar *et al.*, Rev. of Mod. Phys. **78**, 000865 (2006).
  - [4] T.A. Maier *et al.*, Phys. Rev. Lett. **95**, 237001 (2005); T.A. Maier *et al.*, cond-mat/0612579.
  - [5] S. S. Kancharla *et al.*, cond-mat/0508205.
  - [6] A. I. Lichtenstein and M. I. Katsnelson, Phys. Rev. B **62**, R9283 (2000); M. Capone and G. Kotliar, Phys. Rev. B **74**, 054513 (2006).
  - [7] M. Jarrell *et al.*, Europhys. Lett. **56**, 563 (2001); T. D. Stanescu and P. Phillips, Phys. Rev. Lett. **91**, 049901(E) (2003).
  - [8] B. Kyung *et al.*, Phys. Rev B **73**, 165114 (2006).
  - [9] O. Parcollet *et al.*, Phys. Rev. Lett. **92**, 226402 (2004).
  - [10] T. D. Stanescu and G. Kotliar, Phys. Rev. B **74**, 125110 (2006); T. D. Stanescu *et al.*, An. of Phys. **321** 1682 (2006).

- [11] K. Haule and G. Kotliar, cond-mat/0605149.
- [12] M. Le Tacon *et al.*, Natur. Phys. **2**, 537 (2006);
- [13] K. Tanaka *et al.*, Science **314**, 1910 (2006).
- [14] For earlier discussions of related ideas see B. Kyung and A.-M.S. Tremblay, cond-mat/0204500; G. Deutcher, Nature 397, 410 (1999);
- [15] M. Caffarel and W. Krauth, Phys. Rev. Lett. **72**, 1545 (1994).
- [16] A. Damascelli *et al.*, Rev. of Mod. Phys. **75**, 473 (2003).
- [17] M. Civelli *et al.*, Phys. Rev. Lett. **95**, 106402 (2005).
- [18] X.J. Zhou *et al.*, Nature **423**, 398 (2003).
- [19] K. Haule, to be published.
- [20] K. McElroy *et al.*, Phys. Rev. Lett. **94**, 197005 (2005).
- [21] G. Kotliar and J. Liu, Phys. Rev. B **38**, R5142 (1988).
- [22] For a review: P. A. Lee *et al.*, Rev. Mod. Phys. 78, 17-85 (2006).
- [23] T. Valla *et al.*, Science **314**, 1914 (2006).
- [24] A. J. Millis, Science **314**, 1888 (2006).